Geophys. J. Int. (2008) **172,** 383–394 doi: 10.1111/j.1365-246X.2007.03649.x

Non-linear traveltime inversion for 3-D seismic tomography in strongly anisotropic media

Bing Zhou[1] and Stewart Greenhalgh[1,2]

[1]*Department of Physics, Adelaide University, North Terrance, Adelaide,* SA 5005*, Australia. E-mail: bing.zhou@adelaide.edu.au*
[2]*Institute of Geophysics, ETH Zürich,* 8093 *Hönggerberg, Switzerland*

Accepted 2007 October 4. Received 2007 October 4; in original form 2007 April 18

SUMMARY

We have developed two, new non-linear traveltime inversion schemes for 3-D seismic tomography in anisotropic media. They differ from the traditional linearized inversion approach and offer five significant improvements: (1) they are based on an alternative form of the first-order traveltime perturbation equation, derived so as to simplify the inversion formulae and overcome the quasi shear wave singularity problem; (2) robust 3-D ray tracing is employed which enables the simultaneous computation of the first-arrival traveltimes and ray paths for the three body waves (qP, qS_1 and qS_2) in arbitrary anisotropic media; (3) the Jacobian matrix used in the update is based on an efficient computation for a 3-D anisotropic model, so that the inversion is applicable to both weakly and strongly anisotropic situations, unlike most previous approaches which assume weak anisotropy; (4) a local-search, constrained minimization is applied to the non-linear inversion which makes anisotropic tomographic imaging an iterative procedure; (5) there is an option to invert for the elastic moduli directly or the Thomsen parameters directly in heterogenous, tilted transversely isotropic media, using any source–receiver recording geometry. We have examined the imaging capability of the non-linear solver with individual body-wave modes using a 3-D synthetic anisotropic model incorporating two targets, a 'high velocity' and a 'low velocity' anomaly, embedded in a titled transversely isotropic medium. The model is illuminated by means of azimuthal VSP and crosshole measurements. The experimental results show that the two non-linear inversion schemes successfully image the 'targets' and yield satisfactory 3-D tomograms of the elastic moduli and the Thomsen parameters.

Key words: Inverse theory; Tomography; Body waves; Seismic anisotropy.

INTRODUCTION

The usual approach to reconstruct a 3-D image of the subsurface, or the deep structure of the Earth's interior, is seismic traveltime tomography (see e.g. Aki *et al.* 1977; Nolet 1987; Bregman *et al*. 1989; Sambridge 1990; Sehudandi & Toint 1993; Day *et al*. 2001; Zelt *et al*. 2001; Bai & Greenhalgh 2005). Its popularity and appeal stems from the simple physical principle involved, the ease of measurement and the straightforward nature of the data processing. Full 3-D elastic waveform inversion is still in its infancy, can be highly unstable without excellent system calibration and knowledge of the source signal, and is computationally very demanding (Tarantola 1984; Pratt 1999; Pratt & Shipp 1999; Greenhalgh & Zhou 2003; Xu *et al.* 2006). From a theoretical viewpoint, seismic traveltime tomography can be broken down into two parts: (1) kinematic ray tracing in a 3-D geological model and (2) use of a non-linear inversion solver to reconstruct the medium properties (wave speed) from the observed traveltimes of the seismic body waves. The first part, also called forward modelling, calculates the traveltimes and corresponding ray paths traversing the medium for every source–receiver pair. The second part, called the inverse problem, automatically finds a 3-D seismic model, whose synthetic traveltimes optimally match the observed data subject to certain constraints and model smoothness criteria. The inverted 3-D seismic model is then taken to be a physical image of the underground geological situation.

Reviewing all of the 3-D ray tracing used in seismic traveltime tomography, one finds that most employ ray tracing techniques that deal with heterogeneous, isotropic media. This includes the finite difference solvers (Vidale 1990; Kim & Cook 1999; Qian & Symes 2002), the network algorithms (Moser 1991; Klimes & Kvasnička 1994; Cheng & House 1996; Bai & Greenhalgh 2005) and the fast marching method (Sethian & Popovici 1999; Rawlinson & Sambridge 2004). This means that traditional 3-D seismic traveltime tomography is only applicable for imaging an isotropic subsurface in which the wave speeds are independent of the wave-propagation direction. However, in reality, many laboratory studies (Musgrave 1970; Helbig 1981; Crampin 1984; Thomsen 1986) and seismological observations (Anderson & Dziewonski 1982; Tanmoto & Aderson 1985; Nataf *et al.* 1986) show that some rocks and parts of the Earth's interior are distinctly anisotropic. This is

particularly true when the rocks have aligned structures, such as mineral/crystal orientation (Musgrave 1970), fine layering (Helbig 1981) and parallel cracks (Crampin 1984). As is well known, wave propagation in an anisotropic medium differs quite significantly from that in an isotropic medium (Crampin 1981). Three types of body wave (qP, qS_1 and qS_2) instead of two (P, S) propagate in an anisotropic medium and travel at their own wave speeds (both group and phase velocity, which are different), varying with the wave-propagation direction. To image anisotropic media, one should take into account the anisotropic properties so as to make 3-D seismic traveltime tomography applicable for such situations.

To perform seismic traveltime inversion for a general anisotropic medium, Červeny (1982), Červeny & Jech (1982) and Hanyga (1982) developed some fundamental formulae that give the first-order quantitative relationships between the traveltime perturbation and the elastic modulus perturbation (variation) in the medium. Jech & Pšenčik (1989) extended the linearized formulae to overcome the singularity problem when applied to the two quasi shear wave modes (qS_1, qS_2). In the last two decades, these formulae have been successfully applied to the velocity sensitivity analysis of the seismic body waves (Farra & Le Bėgat 1995; Chapman & Miller 1996) and imaging 2-D or 3-D structures in heterogenous anisotropic media (Hirahara & Yuzo 1984; Jech 1988; Chapman & Pratt 1992; Pratt & Chapman 1992; Watanabe *et al.* 1996; Wu & Lees 1999; Eberhart & Henderson 2004; Zheng 2004). From these developments and applications, one finds that there is the common assumption that the media are 'weakly' anisotropic. This implies that the anisotropic media can be treated as a small elastic parameter perturbation from an isotropic background. This is to avoid successive ray tracing in an anisotropic medium and upgrading of the Jacobian matrix after each iteration. They are generally replaced by ray tracing in an isotropic (reference) medium and the use of a constant Jacobian matrix. Obviously, this assumption simplifies the forward modelling and the inverse problem, reducing the determination of the elastic moduli and the imaging the structure of the anisotropic media to a simple linearized inversion. However, such a linearized approach is invalid for 'strongly' anisotropic situations, The non-linear nature of the geophysical inverse problem strictly requires a non-linear solver to obtain accurate results or better images of the anisotropic medium (Menke 1984; Tarantola 1987; Aster *et al*. 2005; Greenhalgh *et al*. 2006). A suitable seismic traveltime tomography scheme for anisotropic media imaging should be applicable to both 'weakly' and 'strongly' anisotropic situations, and successively improve the images by continuously upgrading the Jacobian matrix and iteratively approaching the true ray paths. Unfortunately, such 3-D seismic tomographic imaging for anisotropic media has so far not been well developed for practical applications. It is possible to achieve the goal because a number of researchers have developed various techniques for 3-D ray tracing in an anisotropic medium (Gajewski & Pšenčik 1987; Shearer & Chapman 1988; Vavryčuk 2001; Zhou & Greenhalgh 2005b).

In this paper, we present two non-linear inversion schemes for 3-D seismic traveltime tomography, which have less limitations than the traditional linearized inversion approach for anisotropic media. We have developed a new and more applicable form of the first-order traveltime perturbation equation, which involves computation of the wave speed derivatives and does not necessarily involve calculation of the eigenvectors or polarisation directions of the seismic body waves. Therefore, the singularity problem with the quasi shear waves (Crampin & Yedlin 1981) is completely avoided. For the forward modelling, we employed our newly developed 3-D ray tracer simultaneously to calculate the first-arrival traveltimes and corresponding ray paths for the three seismic body waves (qP, qS_1 and qS_2) in an arbitrary anisotropic medium. For the non-linear inversion, we developed an efficient way to compute the Jacobian matrix for the anisotropic model and implemented local-search, constrained minimization solutions for two distinct inversion schemes—one to obtain the elastic moduli and the other to obtain the Thomsen parameters—for an arbitrary 3-D tilted transversely isotropic medium (TTI-medium). These inversion schemes were examined by imaging the structure of a complex 3-D synthetic model. They satisfactorily recovered the elastic moduli and the Thomsen parameters throughout the rock volume.

FIRST-ORDER TRAVELTIME PERTURBATION EQUATION

Červeny (1982), by solving the ekinoal equation with a Hamiltonian method, obtained the first-order traveltime perturbation equation:

$$\delta\tau = -\frac{1}{2}\int_R p_i p_l g_k g_j \delta a_{ijkl}\frac{\mathrm{d}s}{U}, \tag{1}$$

where a_{ijkl} is the fourth rank tensor of the density-normalized elastic moduli, τ is the traveltime of the seismic wave propagating along the undisturbed ray path R, $\mathbf{p} = (p_1, p_2, p_3)$ and $\mathbf{g} = (g_1, g_2, g_3)$ are the phase-slowness vector and the eigenvector of the Christoffel equation, ds and U stand for a small segment of R and the group velocity, respectively. All of the quantities and vectors in eq. (1) are functions of the spatial coordinates $\mathbf{x}$ of the ray path R, and they are calculated with the undisturbed reference model, which may be an arbitrary anisotropic medium. In eq. (1), we do not explicitly specify the seismic body-wave mode because the equation is valid for all of the three modes (qP, qS_1 and qS_2). Of course, different values of the quantities $\mathbf{p}$, U, $\mathbf{g}$ and τ apply in each case.

As is well known, there can be up to 21 independent components of the fourth-rank modulus tensor (depending on the class of anisotropy), due to the symmetry principle (Musgrave 1970). For general applications, we apply $m_v \in \{a_{ijkl}\}$ to represent the independent elastic moduli and rewrite eq. (1) as follows:

$$\delta\tau = -\frac{1}{2}\int_R \left(\frac{\partial a_{ijkl}}{\partial m_v} p_i p_l g_k g_j\right)\delta m_v \frac{\mathrm{d}s}{U}. \tag{2}$$

To apply eq. (2) one must calculate the eigenvectors of the three wave modes (qP, qS_1 and qS_2). A singularity problem is encountered with the quasi shear waves when their phase velocities, for certain directions of propagation, co-incide (Crampin & Yedlin 1981; Jech & Pšenčik 1989). To simplify eq. (2), we use the equivalent form of eq. (2) obtained by Chapman & Pratt (1992), who applied Fermat's Principle

to obtain:

$$\delta\tau = \int_R \delta\mathbf{p}\cdot \mathrm{d}\mathbf{x}, \tag{3}$$

Here the phase-slowness vector $\mathbf{p} = \mathbf{p}(m_\nu, \mathbf{n})$ is a function of the model parameters m_ν and the phase-slowness direction $\mathbf{n} = (n_1, n_2, n_3)$ (or wave front normal). The perturbation of the phase-slowness vector (i.e. the total differential) may be calculated by expanding out in terms of the partial derivatives in the usual way:

$$\delta\mathbf{p} = \left(\frac{\partial\mathbf{p}}{\partial m_\nu}\right)\delta m_\nu + \left(\frac{\partial\mathbf{p}}{\partial n_q}\right)\delta n_q, \tag{4}$$

Substituting into eq. (3) we see that the first-order traveltime perturbation comprises two parts:

$$\delta\tau = \int_R \left[\hat{\mathbf{r}}\cdot\left(\frac{\partial\mathbf{P}}{\partial m_\nu}\right)\right]\delta m_\nu \mathrm{d}s + \int_R \left[\mathbf{U}\cdot\left(\frac{\partial\mathbf{P}}{\partial n_q}\right)\right]\delta n_q \mathrm{d}\tau. \tag{5}$$

Here, the ray direction $\hat{\mathbf{r}} = \mathrm{d}\mathbf{x}/\mathrm{d}s$ and the group velocity $\mathbf{U} = \mathrm{d}\mathbf{x}/\mathrm{d}\tau$ have been applied. Eq. (5) indicates that the first term on the RHS is the contribution from the model parameter changes δm_ν with a fixed wave front normal $\mathbf{n}$ and the second term represents the contribution from variations of the wave front normal δn_q with unchanged model parameters m_ν. Now the integrand of the second integral can be shown to vanish, since

$$\mathbf{U}\cdot\frac{\partial\mathbf{p}}{\partial n_q} = U_i\frac{\partial}{\partial n_q}\left(\frac{n_i}{c}\right) = U_i\left(\frac{\delta_{iq}}{c} - \frac{n_i}{c^2}\frac{\partial c}{\partial n_q}\right) = \frac{1}{c}(U_q - U_q) = 0, \tag{6}$$

which gives rise to a new version of the first-order traveltime perturbation equation:

$$\delta\tau = \int_R \left[\hat{\mathbf{r}}\cdot\left(\frac{\partial\mathbf{p}}{\partial m_\nu}\right)\right]\delta m_\nu \mathrm{d}s, \tag{7}$$

where the derivatives in the integrand are calculated with a fixed wave front normal $\mathbf{n}$, that is $\mathbf{n} = \mathbf{n}(\mathbf{x})$, $\mathbf{x}\in R$, which is determined by the fixed ray path R with the relationship $\mathbf{n}\cdot\hat{\mathbf{r}} = c(\mathbf{x})/U(\mathbf{x})$, $\mathbf{x}\in R$ and the reference model parameters m_ν. Differentiating both sides of the identity $\mathbf{p}\cdot\mathbf{U} = 1$ (Musgrave 1970), we have the following equation for the integrand of eq. (7):

$$\hat{\mathbf{r}}\cdot\left(\frac{\partial\mathbf{p}}{\partial m_\nu}\right) = -\frac{1}{cU}\left(\mathbf{n}\cdot\frac{\partial\mathbf{U}}{\partial m_\nu}\right). \tag{8}$$

Accordingly, eq. (7) can be rewritten in the following form:

$$\delta\tau = -\int_R \frac{1}{cU}\left[\mathbf{n}\cdot\left(\frac{\partial\mathbf{U}}{\partial m_\nu}\right)\right]\delta m_\nu \mathrm{d}s. \tag{9}$$

With a fixed wave front normal $\mathbf{n} = \mathbf{n}(\mathbf{x})$, $\mathbf{x}\in R$ (see eq. 4), we have the expression of the derivative of the phase velocity (Zhou & Greenhalgh 2005a):

$$\frac{\partial c}{\partial m_\nu} = \mathbf{n}\cdot\left(\frac{\partial\mathbf{U}}{\partial m_\nu}\right), \tag{10}$$

and eq. (9) becomes

$$\delta\tau = -\int_R \frac{1}{cU}\left(\frac{\partial c}{\partial m_\nu}\right)\delta m_\nu \mathrm{d}s. \tag{11}$$

Obviously, eqs (7), (9) and (11) do not explicitly involve the eigenvectors and they are much simpler than eqs (1) or (2) obtained by Červeny (1982). This is due to the introduction of the derivatives. These three equations actually require different derivatives of the wave speeds $\partial c/\partial m_\nu$, $\partial\mathbf{p}/\partial m_\nu$ and $\partial\mathbf{U}/\partial m_\nu$, which play crucial roles in the first-order traveltime perturbation. Therefore, we call them the wave speed-derivative versions of the first-order traveltime perturbation equation. It was shown above that the three new versions are equivalent. To apply these new versions, the key step is to calculate the derivatives of the wave speed. In our previous paper (Zhou & Greenhalgh 2005a), two analytic methods, called the eigenvector and eigenvalue methods, have been developed for a general anisotropic medium and numerically shown to yield consistent results, for example, the derivatives of the phase velocity and group velocity vector may be analytically calculated with the eigenvector formula (Zhou & Greenhalgh 2005a):

$$\frac{\partial c}{\partial m_\nu} = \frac{1}{2c}\frac{\partial a_{ijkl}}{\partial m_\nu}n_i n_l g_k g_j, \tag{12}$$

$$\frac{\partial U_i}{\partial m_\nu} = \frac{\partial a_{ijkl}}{\partial m_\nu}p_l g_j g_k - \frac{U_i}{c}\frac{\partial c}{\partial m_\nu} + (a_{ijkl} + a_{ikjl})p_l\frac{\partial g_j}{\partial m_\nu}g_k, \tag{13}$$

or the eigenvalue formula (Zhou & Greenhalgh 2005a):

$$\frac{\partial c}{\partial m_\nu} = \frac{1}{3c\sqrt[3]{r}}\left(\cos B\frac{\partial r}{\partial m_\nu} + D_\nu\right) + \frac{1}{6c}\frac{\partial A}{\partial m_\nu}, \tag{14}$$

$$\begin{cases} \dfrac{\partial U_1}{\partial m_v} = \left(\dfrac{\partial c}{\partial m_v} \sin\theta + \cos\theta \dfrac{\partial^2 c}{\partial m_v \partial \theta} \right) \cos\varphi - \dfrac{\sin\varphi}{\sin\theta} \dfrac{\partial^2 c}{\partial m_v \partial \varphi}, \\ \dfrac{\partial U_2}{\partial m_v} = \left(\dfrac{\partial c}{\partial m_v} \sin\theta + \cos\theta \dfrac{\partial^2 c}{\partial m_v \partial \theta} \right) \sin\varphi + \dfrac{\cos\varphi}{\sin\theta} \dfrac{\partial^2 c}{\partial m_v \partial \varphi}, \\ \dfrac{\partial U_3}{\partial m_v} = \dfrac{\partial c}{\partial m_v} \cos\theta - \sin\theta \dfrac{\partial^2 c}{\partial m_v \partial \theta}, \end{cases} \tag{15}$$

which do not require the eigenvectors. The quantities r, B, D_v and A in eq. (14) and the second-order derivatives in eq. (15) are functions of the model parameters m_v and the wave front normal $\mathbf{n}$ defined by $\mathbf{n} = (\sin\theta\cos\varphi, \sin\theta\sin\varphi, \cos\theta)$. The explicit expressions can be found in our previous paper (Zhou & Greenhalgh 2005a).

Although the three new versions are mathematically equivalent, they have different computational efficiencies when applied to real data inversions. To apply eq. (9), one has to calculate the derivatives of the group velocity. This requires the derivatives of the eigenvector $\partial g_j/\partial m_v$ (see eq. 13), or the second-order derivatives of the phase velocity $\partial^2 c/\partial m_v \partial\theta$ and $\partial^2 c/\partial m_v \partial\varphi$ (see eq. 15), while eq. (11) only involves scalar computations and no requirement of the eigenvectors and the higher-order derivatives if the eigenvalue formula (eq. 14) is used. This means that the quasi shear wave singularity problem can be circumvented so that eq. (11) becomes superior to the other two. This is a most attractive feature of using the new wave speed-derivative version of the travel time perturbation equation.

INVERSION FOR A 3-D TTI-MEDIUM

The formulations in the previous section are valid for a general anisotropic medium. In this section, we focus on a special class of anisotropy viz a 3-D heterogenous TTI-medium, because it is a common geological model in exploration seismic (Helbig 1994; Tsvankin & Grechka 2006) and in earthquake seismology/deep seismic sounding (Takeuchi & Saito 1972; Anderson & Dziewonski 1982). In a TTI-medium, the two quasi shear wave modes qS_1 and qS_2 become qSV and qSH (Daley & Hron 1977; Thomsen 1986). To image the structure of a 3-D anisotropic model, we divide the model domain (Ω) into $N_\Omega = N_x \cdot N_y \cdot N_z$ cells ($\Omega = \sum_k^{N_\Omega} \partial\Omega_k$), where the integers N_x, N_y and N_z are the numbers of the cells in the three coordinate directions, so that we have a 3-D grid consisting of $N = (N_x + 1) \times (N_y + 1) \times (N_z + 1)$ nodes, and each of the cells has eight sets of the model parameters defined by the density-normalized elastic moduli $\mathbf{m}_v^{(k)} = \{(a_{11}^{(k)}, a_{13}^{(k)}, a_{33}^{(k)}, a_{44}^{(k)}, a_{66}^{(k)}, \theta_0^{(k)}, \varphi_0^{(k)}),\ k = 1, 2, \ldots, 8\}$, or Thomsen parameters ($\mathbf{m}_v^{(k)} = \{(\alpha_0^{(k)}, \beta_0^{(k)}, \varepsilon^{(k)},\ \delta^{*(k)}, \gamma^{(k)}, \theta_0^{(k)}, \varphi_0^{(k)}),\ k = 1, 2, \ldots, 8\}$), at the eight corners. Here $\theta_0^{(k)}$ and $\varphi_0^{(k)}$ are the pair of spherical polar angles giving the orientation direction (inclination and azimuth) of the symmetry axis of the TTI-medium. In a heterogeneous anisotropic model the discrete model parameters vary with the spatial coordinates $x_k = [x_1^{(k)}, x_2^{(k)}, x_3^{(k)}]$. In our previous paper (Zhou & Greenhalgh 2005b), we have already demonstrated a robust ray tracing method to simultaneously calculate the traveltimes and corresponding ray paths for all three body waves (qP, qSV and qSH) in such a discrete model.

After the discretization, the traveltime perturbation given by eq. (11) can be calculated by the piecewise summation over the cells:

$$\begin{aligned} \delta\tau &= -\sum_k^{N_\Omega} \int_{R_k} \frac{1}{cU} \left(\frac{\partial c}{\partial m_v} \right) \delta m_v \mathrm{d}s \\ &\approx -\sum_k^{N_\Omega} \frac{R_k}{2} \left[\left(\frac{1}{cU} \frac{\partial c}{\partial m_v} \right)_{x_A^{(k)}} + \left(\frac{1}{cU} \frac{\partial c}{\partial m_v} \right)_{x_B^{(k)}} \right] \delta m_v, \end{aligned} \tag{16}$$

where R_k is the segment of the ray path R in the kth cell $\partial\Omega_k$ and $\mathbf{x}_A^{(k)}$ and $\mathbf{x}_B^{(k)}$ are the two endpoints of R_k traversing the cell. Eq. (16) shows that the calculation requires the three quantities c, U and $\partial c/\partial m_v$ at the two endpoints, for which we apply the Lagrange interpolation formula:

$$\begin{pmatrix} c(\mathbf{x}) \\ U(\mathbf{x}) \\ \partial c(\mathbf{x})/\partial m_v \end{pmatrix} = \sum_{i=1}^{8} \prod_{\substack{l=1 \\ l \neq i}}^{8} \left[\frac{(\mathbf{x} - \mathbf{x}_l^{(k)})}{(\mathbf{x}_i^{(k)} - \mathbf{x}_l^{(k)})} \right] \begin{pmatrix} c(\mathbf{x}_i^{(k)}) \\ U(\mathbf{x}_i^{(k)}) \\ \partial c(\mathbf{x}_i^{(k)})/\partial m_v \end{pmatrix}, \ \mathbf{x},\ \mathbf{x}_i^{(k)} \in \Omega_k \tag{17}$$

The nodal values $c(\mathbf{x}_i^{(k)})$, $U(\mathbf{x}_i^{(k)})$ and $\partial c(\mathbf{x}_i^{(k)})/\partial m_v$ may be calculated by the analytic methods described in our paper (Zhou & Greenhalgh 2005a), using the undisturbed model parameters $\mathbf{m}_v^{(k)}$.

Applying eq. (16) to a large number of ray paths leads to the following matrix form of equation for non-linear inversion (Zhou *et al*. 1992; Greenhalgh *et al*. 2006):

$$\mathbf{m}_{q+1} = \mathbf{m}_q + Z_m \left[\left(\mathbf{J}_q^T \mathbf{W}_d \mathbf{J}_q + \lambda \mathbf{W}_m \right)^{-g} \mathbf{J}_q^T \mathbf{W}_d \delta\tau_{\mathbf{q}}, \quad (q = 1, 2, \ldots.), \right. \tag{18}$$

where the subscript '$-g$' stands for the generalized inverse matrix, the operators $\mathbf{W}_d$ and $\mathbf{W}_m$ are the weighting matrices for the data and the model parameters, respectively, both of which can be chosen in terms of the available information on the data noise and the model variation (Menke 1984; Tarantola 1987; Carrion 1989). The real scalar λ is a trade-off parameter between the data fit and the degree of model

perturbation, and the other quantities are given by

$$\delta\tau = \left\{\tau_j^{ob} - \tau_j^{syn}(\mathbf{m}_q), \quad j = 1, 2, \ldots M\right\},$$
$$\mathbf{m}_q = \left\{m_{v_k}^{(q)}, \quad k = 1, 2, \ldots, N\right\},$$
$$Z_m(m_v) = \{a_v \le m_v \le b_v\},$$
$$\mathbf{J}_q = \left(\frac{\partial \tau_j}{\partial m_{v_i}^{(q)}}\right)_{M\times N}, \tag{19}$$

where τ_j^{ob} and $\tau_j^{syn}(\mathbf{m}_q)$ are the observed and synthetic traveltimes along the jth ray path and Z_m is the constraint operator defined by the lower and upper bounds $[a_v, b_v]$ for each inverted parameters m_v, and $\mathbf{J}_q$ is the Jacobian matrix calculated by the following formula:

$$\frac{\partial \tau_j}{\partial m_{v_i}^{(q)}} = -\sum_k^{N_\Omega} \frac{R_{jk}^{(q)}}{2}\left[\left(\frac{1}{cU}\frac{\partial c}{\partial m_{v_i}^{(q)}}\right)_{\mathbf{x}_{A_j}^{(q)}} + \left(\frac{1}{cU}\frac{\partial c}{\partial m_{v_i}^{(q)}}\right)_{\mathbf{x}_{B_j}^{(q)}}\right]. \tag{20}$$

It should be noted that the summation in the above equation counts the cells that the particular ray path R_j traverses $[R_{jk}^{(q)} \neq 0]$, which is generally a small number compared to the total number of cells in the model. This means that the Jacobian matrix generally has large dimensions and a sparse pattern, making it suitable to use an iterative solver, such as the conjugate gradient method (Zhou *et al*. 1992, Greenhalgh *et al*. 2006), for the generalized inverse matrix in eq. (18). We also should point out that there are two options for the derivatives in eq. (20). One is to use the derivatives with respect to the elastic moduli, e.g. derivatives $\partial c/\partial m_v$, $m_v \in \{a_{11}, a_{13}, a_{33}, a_{44}, a_{66}\}$, which are calculated with the analytic expressions of the phase velocities given by Daley & Horn (1977) or Thomsen (1986), and the other is to apply the derivatives with respect to the Thomsen parameters (α_0, β_0, ϵ, δ^*, γ), that is,,

$$\begin{cases}
\dfrac{\partial c}{\partial \alpha_0} = 2\alpha_0(2\varepsilon+1)\dfrac{\partial c}{\partial a_{11}} + \dfrac{\alpha_0\left[\alpha_0^2(\varepsilon+\delta^*+1) - \beta_0^2(\varepsilon+2)\right]}{\left(a_{13}+\beta_0^2\right)}\dfrac{\partial c}{\partial a_{13}} + 2\alpha_0\dfrac{\partial c}{\partial a_{33}}, \\
\dfrac{\partial c}{\partial \beta_0} = \left\{\dfrac{\beta_0[2\beta_0^2 - \alpha_0^2(\varepsilon+2)]}{\left(a_{13}+\beta_0^2\right)} - 2\beta_0\right\}\dfrac{\partial c}{\partial a_{13}} + 2\beta_0\dfrac{\partial c}{\partial a_{44}} + 2\beta_0(2\gamma+1)\dfrac{\partial c}{\partial a_{66}}, \\
\dfrac{\partial c}{\partial \varepsilon} = 2\alpha_0^2\dfrac{\partial c}{\partial a_{11}} + \dfrac{\alpha_0^2\left[\alpha_0^2-\beta_0^2\right)\right]}{2\left(a_{13}+\beta_0^2\right)}\dfrac{\partial c}{\partial a_{13}}, \\
\dfrac{\partial c}{\partial \delta^*} = \dfrac{\alpha_0^4}{2\left(a_{13}+\beta_0^2\right)}\dfrac{\partial c}{\partial a_{13}}, \\
\dfrac{\partial c}{\partial \gamma} = 2\beta_0^2\dfrac{\partial c}{\partial a_{66}}.
\end{cases} \tag{21}$$

which are obtained by the differential chain rule. This leads to two inversion schemes which may be used to image the structures, such as spatial variations in the elastic moduli or the Thomsen parameters. We call the two inversion schemes the elastic modulus scheme and the Thomsen parameter scheme.

So far, we have not specified a body-wave mode in the above formulations in that they are all applicable for the three body-wave modes (qP, qSV and qSH). To discriminate them, we adapted the explicit expressions of the phase velocities given by Daley & Hron (1977) or Thomsen (1986) for a TTI-medium. We have numerically shown that these expressions may give two independent slowness sheets for the two quasi shear waves even when they cross, so that we can easily identity the wave modes in the computations (Zhou & Greenhalgh 2004).

SYNTHETIC EXPERIMENTS

In order to test the imaging capability of the new non-linear inversion schemes, we wrote a PC program *3-Dray_gTI* (it may be download from the website: www.adelaide.edu.au/directory/bing.zhou) and designed a 3-D anisotropic model shown in Fig. 1. This model is of volume, 50 m × 50 m × 50 m and has 121 geophones distributed uniformly over the upper surface, plus an additional 40 geophones in the four boreholes (10 geophones in each hole, spaced at 5 m intervals). Two isolated prismatic 'targets' are placed in the background medium at depths of 10 m and at different horizontal locations. Each body is 10 m thick and of lateral dimension 10 m. The background medium and the two 'targets' are anisotropic rocks, each having 45°-dipping symmetry axes. Their Thomsen parameters are listed in Fig. 1 and they were obtained from laboratory measurements (Thomsen 1986), from which it can be appreciated that all three rocks are strongly anisotropic. One of the 'targets' is a 'high velocity' body while the other is a 'low velocity' body. To image the two 'targets', 10 sources were successively fired in each borehole (at 5 m intervals, co-inciding with the geophone locations) and recorded on all surface geophones and the 30 geophones located in the other three boreholes (the geophones in the source hole were not used). The shooting procedure was repeated for all four holes, yielding in total 6040 traveltimes for every body-wave mode. With this synthetic model, we applied our 3-D ray tracing method (Zhou & Greenhalgh 2005b) and accurately calculated the traveltimes of the three wave modes (qP, qSV and qSH). To the resulting synthetic traveltimes was added Gaussian random noise of level <5 per cent (standard deviation) to produce the 'observed' data as input to the inversion routines. Both 'isotropic' and 'anisotropic' inversions were performed for each individual wave mode. The former treated the model as composite isotropic media and

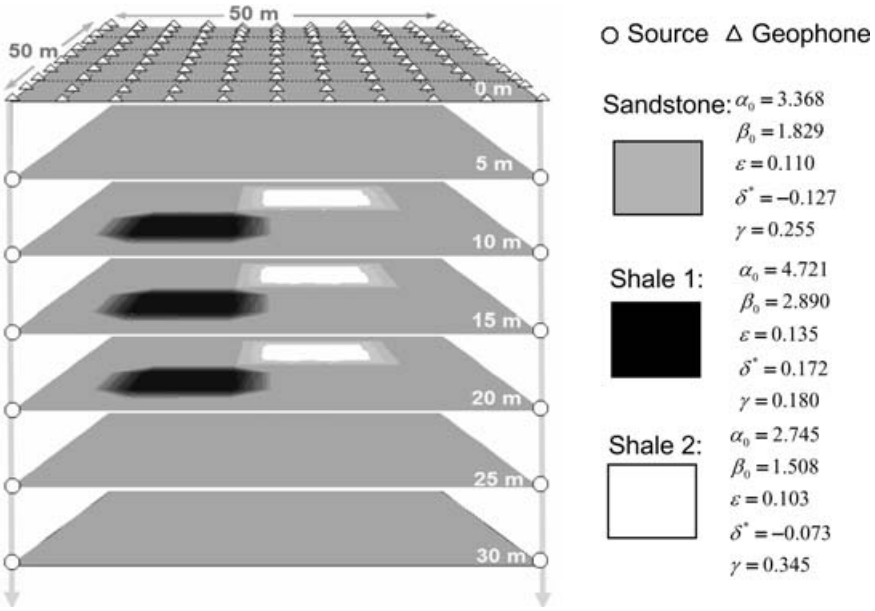

Figure 1. Synthetic anisotropic model for the numerical experiments of 3-D seismic traveltime tomography. The Thomsen parameters of the three rocks are adopted from the Laboratory measurements given by Thomsen (1986).

used a traditional seismic traveltime tomography algorithm (Zhou *et al*. 1992) to reconstruct the *P*- and *S*-wave velocity structures ($V_{\rm p}$, $V_{\rm S}$). The latter applied the traditional linearized anisotropic inversion (weak anisotropy assumption) and the new non-linear anisotropic inversion described in the previous section. The linearized anisotropic inversion used the isotropic reference model computed by $a_{11}^{\rm iso} = a_{33}^{\rm iso} = 0.5(a_{11} + a_{33})$, $a_{44}^{\rm iso} = a_{66}^{\rm iso} = 0.5(a_{44} + a_{66})$, and $a_{13}^{\rm iso} = a_{11}^{\rm iso} - 2a_{44}^{\rm iso}$ and a constant Jacobian matrix. The non-linear anisotropic inversion entailed both the elastic modulus scheme and the Thomsen parameter scheme, which iteratively upgrade the ray paths, the Jacobian matrix and the anisotropic media. For all of the synthetic non-linear inversion experiments, we started with a homogeneous medium (isotropic or anisotropic, respectively), set the unit matrix as the weighting operator in each case $\mathbf{W}_d = \mathbf{I}$ and $\mathbf{W}_{\boldsymbol{m}} = \mathbf{I}$, and implemented the iterative inversions given by eq. (18) until the data fit reached a satisfactory level with an optimal regularisation or damping parameter ($\lambda \in 0.001 \sim 10.0$).

Fig. 2 gives the results of the linearized anisotropic inversion for all three wave modes (qP, qSV and qSH). These results show that the 'high velocity' anomaly is distorted, the 'low velocity' body is hardly seen and many artificial anomalies appear in the shallow and deep parts of the target field as a result of ignoring the strongly anisotropic nature of the rocks and the non-linear nature of the inverse problem.

Fig. 3 gives the results of the isotropic inversion (Fig. 3a) and the non-linear anisotropic inversion (Figs 3b and c) with the qP-wave data. From these results it can be seen that the isotropic inversion is unable to reconstruct clear images of the two targets because the prevalent anisotropy of the media is ignored. The isotropic inversion almost loses the image of the 'low velocity' body (Shale 2) and produces many spurious anomalies in the deeper parts of the model. Implementing the Thomsen parameter scheme of the non-linear anisotropic inversion, we obtained the tomograms of the three parameters: α_0, ε and δ^* (see Fig. 3b), which are the dominant parameters for this wave mode and for this recording geometry. Although the inverted ϵ distribution is not as good as expected, the results for the other two parameters are much better than with the isotropic inversion (see Fig. 3a) and the linearized anisotropic inversion (see Fig. 2). In particular, one can see that the α_0 tomogram successfully recovers the two 'targets' with the right sizes and locations and the inverted δ^* gives a good image of the 'high velocity' body (Shale 1). These imaging differences are mainly caused by the incomplete illumination with the given measurement configuration (lack of vertical ray paths) and the sensitivity behaviour of the Thomsen parameters to the qP-wave velocity (Zhou & Greenhalgh 2005a). The three parameters are actually dominant for the wave speed changes of the qP-wave, but α_0 is almost 'isotropic' among the three, or much less anisotropic than other two. Since ϵ and δ^* are strongly sensitive to the ray path directions, this means that with a certain coverage of ray paths, or a specified recording configuration, the inversion result for α_0 should be much better than the other two, because it does not seriously depend on the ray path directions like the parameters δ^* and ϵ do. Fig. 3(b) is clear confirmation of this. Implementing the elastic modulus scheme of the non-linear anisotropic inversion, we obtained the tomograms for four elastic moduli: a_{11}, a_{13}, a_{33} and a_{44} (see the upper row in Fig. 3c). The four reconstructions clearly give the images of the two 'targets' in the depth range of 10–20 m and verify the superiority of the non-linear anisotropic inversion to the linearized anisotropic inversion. From the inverted moduli, one can calculate the Thomsen parameters (we call them the converted Thomsen parameters) using the well-known relationships: $\alpha_0 = \sqrt{a_{33}}$ and $\beta_0 = \sqrt{a_{44}}$ (see the lower row in Fig. 3c). Comparing the converted Thomsen parameters with those obtained directly by the Thomsen parameter scheme (Fig. 3b), we find that the converted Thomsen parameters are not as good. Specifically, the result for α_0 from the Thomsen parameter inversion scheme is much better than the converted one from the elastic modulus inversion scheme. It can be explained as follows: α_0 behaves as an 'isotropic' parameter in the former while in the latter the elastic modulus $a_{33}(= \alpha_0^2)$ is more sensitive to certain ray path directions (Zhou & Greenhalgh 2005a). Another cause may be that minor errors in the four inverted elastic moduli get amplified or mixed up in the conversion so that the converted

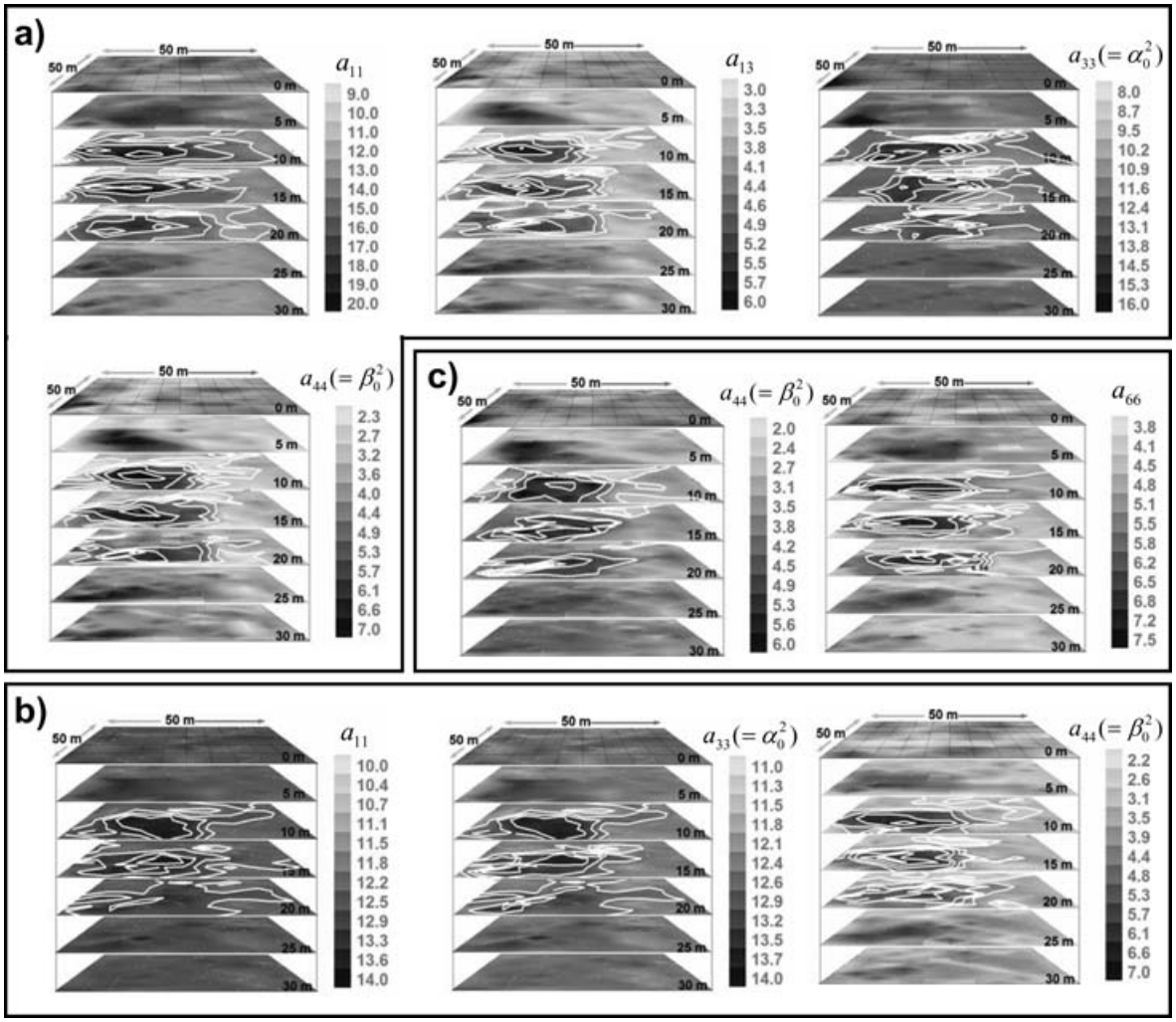

Figure 2. Results of the linearized anisotropic inversions with the (a) qP-wave, (b) qSV-wave and (c) qSH-wave data.

Thomsen parameters are worse than the results of the direct Thomsen parameter scheme. It is also apparent that with the qP-wave data, the Thomsen parameter scheme of the non-linear anisotropic inversion cannot give a good image of β_0 because of the much weaker effects it has than any other parameters on this wave mode (Zhou & Greenhalgh 2005a). However, the elastic modulus scheme of the non-linear anisotropic inversion can successfully recover the structure of the 'shear wave-related' parameter with the qP-wave data.

Fig. 4 gives the results of the isotropic inversion (Fig. 4a) and non-linear anisotropic inversion (Figs 4b and c) with the qSV-wave traveltimes, from which we see that the isotropic inversion produces a distorted image for the 'high velocity' body (Shale 1) and fails to indicate the existence of the 'low velocity' block (Shale 2). By contrast, the Thomsen parameter scheme of the non-linear anisotropic inversion yields clear images for both 'targets' in the β_0 and δ^* tomograms (see Fig. 4b), which are the dominant parameters of the qSV wave. The elastic modulus scheme of the non-linear inversion produces three satisfactory tomograms of a_{11}, a_{33} and a_{44} (the upper row in Fig. 4c), all of which correctly indicate the sizes and positions of the two anomalous blocks. From the inverted elastic moduli, we also obtained the converted Thomsem parameters including α_0 (the lower row in Fig. 4c), which cannot be resolved by the Thomsen parameter scheme with the qSV-wave data due to the weak effects it has on this wave mode. Obviously, the two non-linear anisotropic inversion schemes are much better than the isotropic inversion and the linearized anisotropic inversion when applied to the strongly anisotropic media. However, the converted β_0 and δ^* (the lower row in Fig. 4c) are not as good as the results obtained directly by the Thomsen parameter inversion scheme (see Fig. 4b). It once again shows that the conversion process amplifies or compounds minor discrepancies in the inverted elastic moduli so that they mask the two targets in the converted Thomsen parameter tomograms.

Fig. 5 shows the results obtained by the isotropic inversion (Fig. 5a) and the non-linear anisotropic inversions (Figs 5b and c) with the qSH-wave traveltimes. Again, the isotropic inversion yields distorted and incomplete images of the two 'targets' and produces many fictitious anomalies (see Fig. 5a). The Thomsen parameter scheme of the non-linear anisotropic inversion successfully recovers the spatial variations in β_0, giving the correct dimensions, locations and magnitudes of the two 'targets' (see Fig. 5b). Theoretically, there are only two Thomsen parameters β_0 and γ, or elastic moduli a_{44} and a_{66}, which play a role in the wave speeds for the qSH wave mode. Unfortunately, the Thomsen

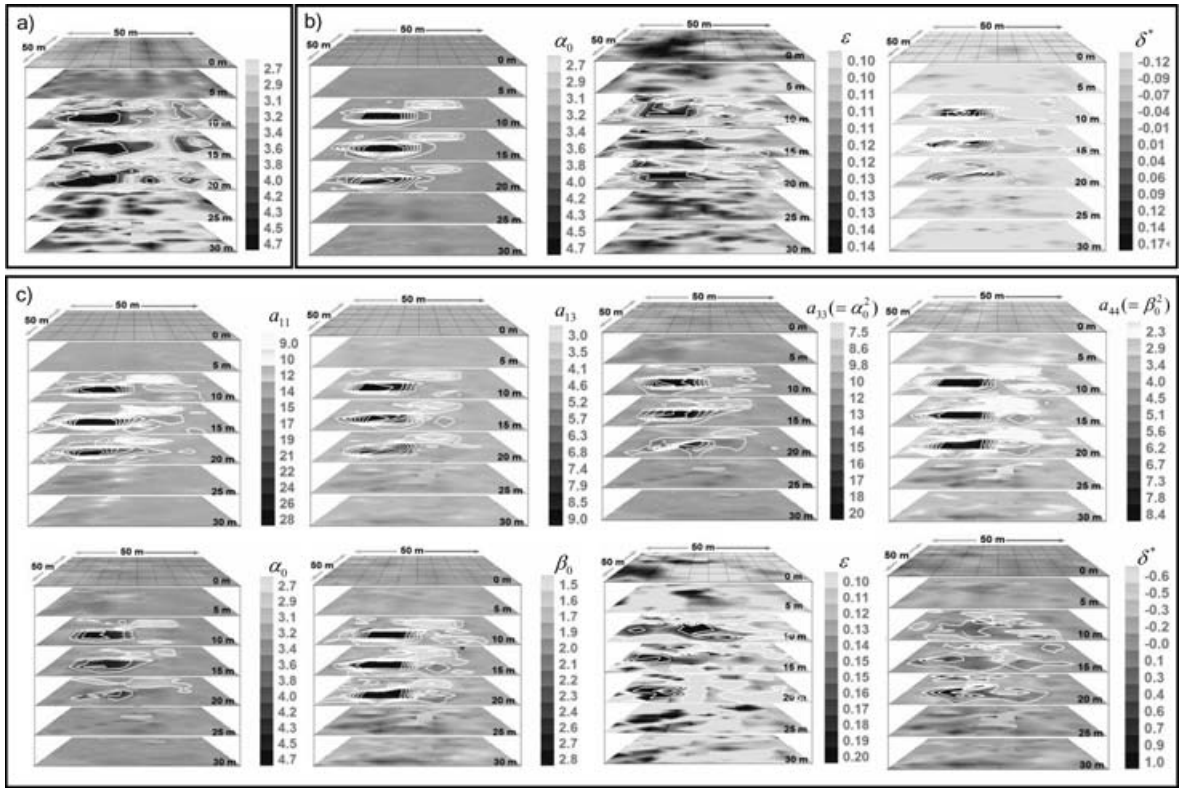

Figure 3. Results of the (a) isotropic inversion and two non-linear anisotropic inversions: (b) Thomsen parameter scheme and (c) elastic module scheme with the qP-wave traveltimes. Thomsen parameter scheme successfully yields the α_0- and δ^*-image, and the elastic modulus scheme recovers the structures very well for all four elastic moduli (a_{11}, a_{13}, a_{33}, a_{44}); both non-linear inversion schemes are obviously superior to the isotropic and linearized anisotropic inversions (Fig. 2a).

parameter scheme is unable to give a reasonable tomogram of γ, which is mainly sensitive to a certain range of the ray directions. For example, in the VTI case γ is most sensitive to the vertical ray paths (Zhou & Greenhalgh 2005a), which are lacking in the measurement configuration used in this experiment. However, implementing the elastic modulus scheme of the non-linear anisotropic inversion, we obtained satisfactory tomograms of a_{44} and a_{66}, both of which correctly define the sizes and depth ranges of the two 'targets' (see Fig. 5c). The images are obviously much better than those obtained by isotropic inversion (Fig. 5a) and the linearized anisotropic inversion (see Fig. 2c), and competitive with the results of the direct Thomsen parameter scheme (see Fig. 5b). Applying the two inverted elastic moduli, we calculated the tomogram of γ [$= (a_{66} - a_{44})/2a_{44}$, which unfortunately cannot delineate the 'targets' from the conversion (not shown). This is believed to be due to compounding of inversion errors.

To assess the degree of data fit with the three types of inversions (isotropic, linearized and non-linear anisotropic inversions), we present in Table 1 the root-mean-square (rms) traveltime residuals at the initial and 20th iteration for all three modes. The table clearly shows that the non-linear anisotrotpic inversion is far superior and reaches a satisfactory convergence level, whereas the other two do not.

CONCLUSIONS

We presented two new non-linear inversion schemes, called the elastic modulus scheme and the Thomsen parameter scheme, for 3-D seismic traveltime tomography in an arbitrary TTI-medium. These two schemes are based on a newly developed robust 3-D ray tracer that can simultaneously calculate the first-arrival traveltimes and corresponding ray paths in an arbitrary TTI-medium, and a new version of the first-order traveltime perturbation equation. This approach differs from the traditional linearized anisotropic inversion (weak anisotropy assumption) and simplifies the non-linear inversion formulae by introducing the wave speed derivatives with respect to the elastic moduli or the Thomsen parameters. These derivatives may be calculated in the manner of the eigenvalue formulation and applied to assembling the Jacobian matrix with an arbitrary anisotropic background medium. The eigenvectors of the three wave modes (qP, qS_1 and qS_2) or (qP, qSV and qSH) are not required so the new scheme essentially avoids the quasi shear wave singularity problem and is applicable for both 'weakly' and 'strongly' anisotropic situations.

The synthetic imaging experiments show the need for anisotropic inversion when the medium is anisotropic and that better images can be obtained by the non-linear anisotropic inversion than with the linearized anisotropic inversion for a strongly anisotropic case. The two

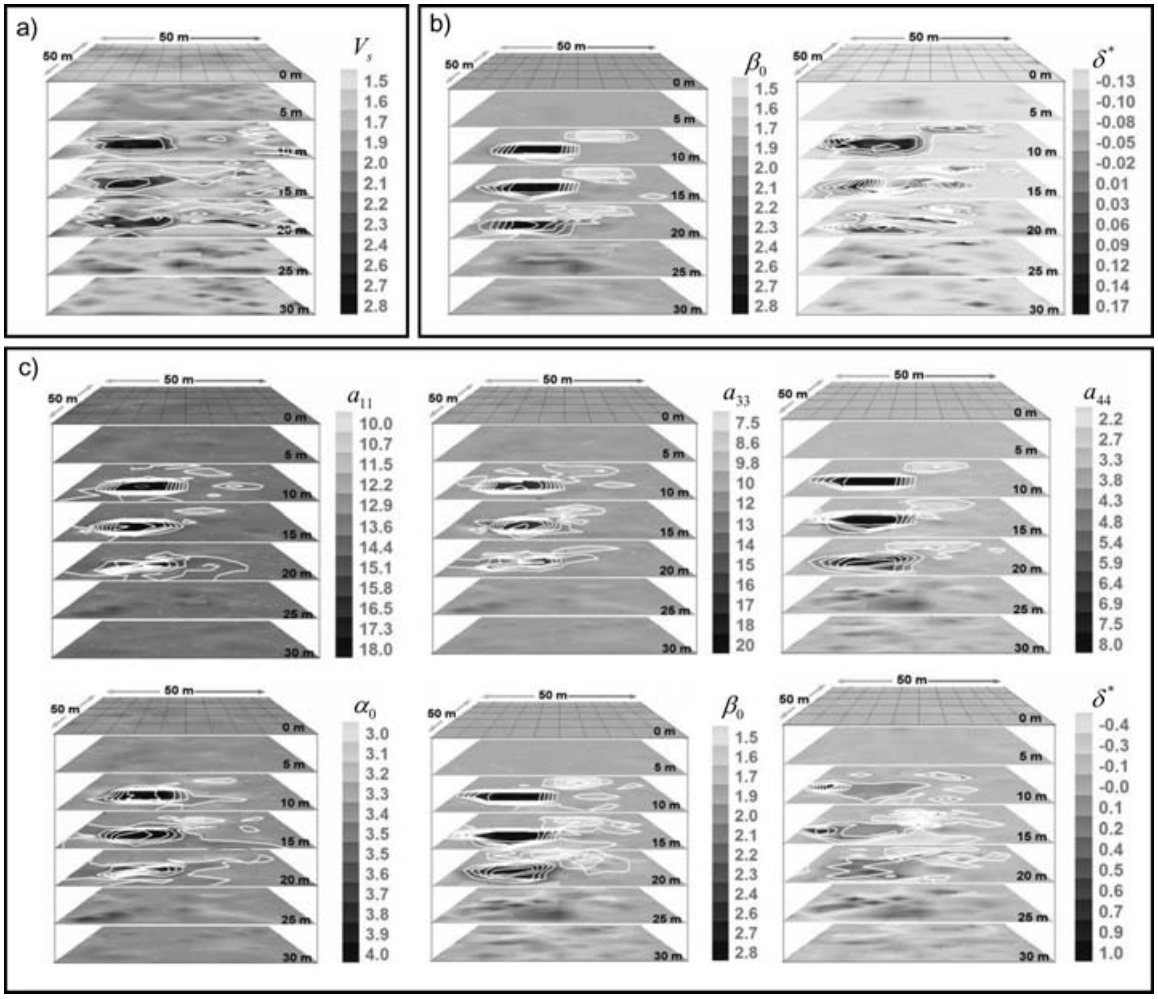

Figure 4. Results of the (a) isotropic inversion and two non-linear anisotropic inversions: (b) Thomsen parameter scheme and (c) elastic modulus scheme with qSV-wave traveltimes. The two non-linear inversion schemes successfully reconstruct the positions and shapes of the two anomalies in the β_0- and a_{44}-tomograms, which are distorted with the isotropic and linearized inversions (Fig. 2b). For the other model parameters, the non-linear inversions are still better than the linearized inversion, even though there is less sensitivity to these parameters than to β_0 and a_{44} in such surveying geometry.

new schemes of the non-linear anisotropic inversion successfully image the 'targets' embedded in a TTI-medium and satisfactorily obtain the Thomsen parameters and the elastic moduli of the TTI-medium. However, the results also show that the two non-linear inversion schemes are not equivalent in imaging the structure of the TTI-medium. This discrepancy is mainly caused by the significant difference in the sensitivity behaviour of the Thomsen parameters and the elastic moduli to the ray directions.

The Thomsen parameter scheme may successfully yield the tomograms of α_0 and β_0 with the qP-wave and one of the two quasi shear wave modes (qSV, qSH), respectively, because of their nearly 'isotropic' properties to the body-wave modes. For the other parameters, such as ε, δ^* and γ, the non-linear anisotropic inversions depend on the distribution of ray directions in the background medium, which in turn depends on the recording geometry. These parameters, are mostly sensitive to a certain range of ray directions. Any lack of these ray directions, or deficiencies in angles of illumination, may cause incomplete or corrupted images for these particular Thomsen parameters. In general, the better the ray path coverage across the target field then the better the image quality and the more Thomsen parameters that may be satisfactorily obtained.

The elastic modulus scheme of the non-linear anisotropic inversion may be applied to the determination of the elastic moduli with an appropriate measurement configuration, that is, VSP + crosshole, and the first-arrival traveltimes of the body-wave modes (qP, qSV and qSH). However, the coverage of ray directions determined by the measurement configuration, and the nature of the background medium, mainly control the resolution of the elastic moduli. They have complementary sensitivity ranges over the ray directions. An incomplete or fragmentary set of ray directions in the survey geometry may result in a loss of recovery of certain elastic moduli which are mostly sensitive to these missing directions. The converted Thomsen parameters from the inverted elastic moduli are generally not as good as those obtained directly by the Thomsen parameter inversion scheme. The main reason is the propagation of inversion errors in the individual elastic moduli, which mask or distort the true images of the structures of the Thomsen parameters.

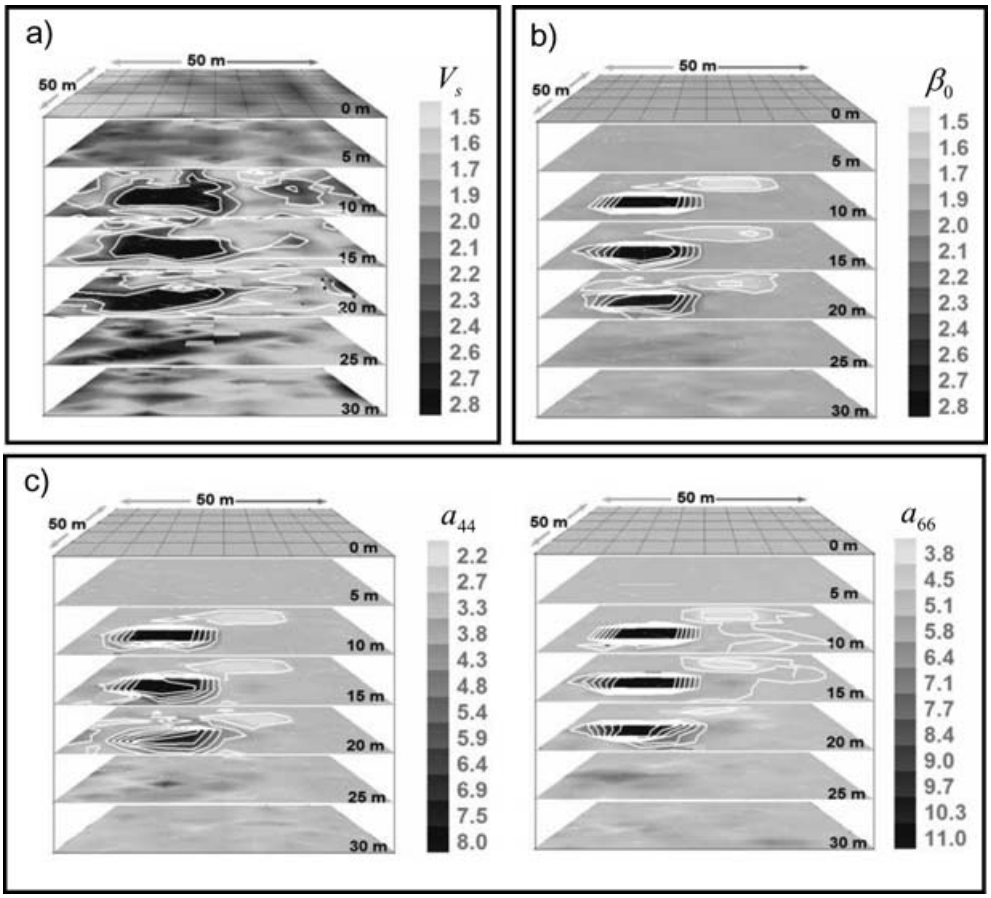

Figure 5. Results of the (a) isotropic inversion and two non-linear anisotropic inversions: (b) Thomsen parameter scheme and (c) elastic modulus scheme with the qSH-wave traveltimes. The two non-linear inversions successfully recover the structure of the two anomalies, which are distorted in the isotropic and linearized inversions (Fig. 2c).

Table 1. The rms traveltime residuals of the three types of inversions for all three wave modes.

Isotropic inversion		
Wave mode	Travel time initial	Residual (rms, ms) 20th iteration
qP	1.292	0.352
qSV	2.222	0.299
qSH	4.619	0.574

Linearized anisotropic inversion		
Wave mode	Travel time initial	Residual (rms, ms) final
qP	0.921	0.282
qSV	1.748	0.650
qSH	2.403	0.550

Non-linear anisotropic inversion		
Wave mode	Travel time initial	Residual (rms, ms) 20th iteration
qP	0.724	0.011
qSV	1.617	0.036
qSH	1.429	0.016

ACKNOWLEDGMENTS

This research was supported by a grant from the Australian Research Council. The authors greatly appreciate the comments made by the two reviewers, Dr Mirko van der Baan and Dr Nick Rawlinson, to improve the paper.

REFERENCES

Aki, K., Christofferson, A. & Husebye, E., 1977. Determination of the three-dimensional seismic structure of the lithosphere, *J. geophys. Res.,* **82,** 277–296.

Anderson, D.L. & Dziewonski, A.M., 1982. Upper mantle anisotropy: evidence from free oscillation, *Geophys. J. R. Astr. Soc.,* **69,** 383–404.

Aster, R.C., Borches, B. & Thurber, C.H., 2005. *Parameter Estimation and Inverse Problems*. Elsevier, Amsterdam.

Bai, C.-Y. & Greenhalgh, S.A., 2005. 3-D nonlinear travel-time tomography: imaging high constrast velocity anomalies, *Pure Appl. Geophys.,* **162,** 2029–2049.

Bregman, N.D., Bailey, R.C. & Chapman, C.H., 1989. Determination of the three dimensional seismic structure of the lithosphere, *J. geophys. Res.,* **28,** 277–296.

Carrion, P.M., 1989. Generalized non-linear elastic inversion with constraints in model and data spaces, *Geophys. J.,* **96,** 151–162.

Červeny, V., 1972. Seismic rays and ray intensities in inhomogenous anisotropic media, *Geophys. J. R. Astr. Soc.,* **29,** 1–13.

Červeny, V., 1982. Direct and inverse kinematic problems for inhomogeneous anisotropic media – linearized approach, *Contr. Geophys. Inst. Slov. Aca. Sci.,* **13**. 127–133.

Červeny, V. & Firbas, P., 1984. Numerical modelling and inversion of traveltimes of seismic body waves in inhomogeneous anisotropic media, *Geophys. J.R. Astr. Soc.,* **76,** 41–51.

Červeny, V. & Jech, J., 1982. Linearized solutions of kinematic problems of seismic body waves in inhomogeneous slightly anisotropic media, *J. Geophys.,* **51,** 96–104.

Chapman, C.H. & Miller, D.E., 1996. Velocity sensitivity in transversely isotropic media, *Geophys. Prospect.,* **44,** 525–549.

Chapman, C.H. & Pratt, R.G., 1992. Traveltime tomography in anisotropic media – I Theory, *Geophys. J. Int.,* **109,** 1–19.

Cheng, N. & House, L., 1996. Minimum traveltime calculations in 3-D graph theory, *Geophysics,* **61,** 1895–1898.

Crampin, S., 1981. A review of wave motion in anisotropic and cracked elastic-media, *Wave Motion,* **3,** 343–391.

Crampin, S., 1984. Effective anisotropic constants for wave-propagation through cracked solids, *J. Roy. Astr. Soc.,* **76,** 135–145.

Crampin, S. & Yedlin, M., 1981. Shear-wave singularities of wave propagation in anisotropic media, *J. Geophys.,* **49,** 43–46.

Daley, P.F. & Hron, F., 1977 Reflection and transmission coefficients for transversely isotropic media, *Bull. seism. Soc. Am.,* **67,** 661–675

Day, A.J., Peirce, C. & Sinha, M.C., 2001. Three-dimensional crustal structure and magma chamber geometry at the intermediate-spreading, back-arc Valu Fa Ridge, Lau Basin – results of s wide-angle seismic tomographic inversion, *Geophys. J. Int.,* **146,** 31–52.

Eberhart-Philips, D. & Henderson, C.M., 2004. Including anisotropy in 3-D velocity inversion and application to Marlborough, New Zealand, *Geophys. J. Int.,* **156,** 237–254.

Farra, V. & Le Bėgat, S., 1995. Sensitivity of qP-wave traveltimes and polarization vector to heterogeneity, anisotropy, and interfaces, *Geophys. J. Int.,* **121**, 371–384.

Gajewski, D. & Pšenčik, I., 1987. Computation of high-frequency seismic wavefields in 3-D lateral inhomogenous, anisotropic media, *Geophys. J. R. Astro. Soc.,* **91,** 383–411.

Greenhalgh, S.A. & Zhou, B., 2003. Surface seismic imaging with multi-frequency full-waveform inversion, *Explor. Geophys.,* **34,** 217–224.

Greenhalgh, S.A., Zhou, B. & Green, A., 2006. Solutions, algorithms and inter-relations for local minimization search geophysical inversion, *J. Geophys. Eng.,* **3,** 101–113.

Hanyga, A., 1982. The kinematic inversion problem for weakly laterally inhomogenous anisotropic media, *Tectonophysics,* **90,** 253–262.

Helbig, K., 1981. Systematic classification of layered-induced transverse isotropy, *Geophys. Prospect.,* **29,** 550–577.

Helbig, K., 1994. Foundations of anisotropy for exploration seismics, in *Handbook of Geophysical Exploration Section I. Seismic Exploration*, eds Helbig, K. & Treitel, S., Pergamon, Oxford.

Hirahara, K. & Ishikawa, Y., 1984. Traveltime inversion for three-dimentonal P-wave velocity anisotropy, *J. Phys. Earth,* **32,** 197–218.

Jech, J., 1988. Three-dimensional inverse problem for inhomogeneous transversely isotropic media, *Stud. Geophys. Geod.,* **32,** 136–143.

Jech, J. & Pšenčik, I., 1989. First-order perturbation method for anisotropic media, *Geophys. J. Int.,* **99,** 369–376.

Kim, S. & Cook, R., 1999. 3D traveltime computation using second-order ENO scheme, *Geophysics,* **64**, 1867–1876.

Klimes, L. & Kvasnicka, M., 1994. 3-D network ray tracing, *Geophys. J. Int.,* **116,** 726–738.

Menke, W., 1984. *Geophysical Data Analysis: Discrete Inverse Theory*, Academic Press, Inc, London.

Moser, T.J., 1991. Shortest path calculation of seismic rays, *Geophysics,* **56,** 59–67.

Muagrave, M.J.P., 1970. *Crystal Acoustic, Introduction to the Study of Elastic Waves and Vibrations in Crystals*, Holden-Day, San Freancisco.

Nataf, H.C., Nakanish, D.L., Aderson, D.L., 1986. Measurement of mantle wave velocities and inversion of mantle velocities and inversion for lateral heterogeneities and anisotropy 3. Inversion, *J. geophys. Res.,* **91,** 7261–7307.

Nolet, G., 1987. *Seismic Wave Propagation and Seismic Tomography, in 'Seismic Tomography with Applications in Global Seismology and Exploration Geophysics'*, D. Reidel Publ. Co, Dordrecht, Holland.

Pratt, R.G., 1999. Seismic waveform inversion in the frequency-domain, Part 1: theory and verification in a physical scale model, *Geophysics,* **64,** 888–901.

Pratt, R.G. & Chapman, C.H., 1992. Traveltime tomography in anisotropic media – II Application, *Geophys. J. Int.,* **109,** 20–37.

Pratt, R.G. & Shipp, R.M., 1999. Seismic waveform inversion in the frequency-domain, Part 2: Fault delineation in sediments using crosshole data, *Geophysics,* **64,** 902–914.

Qian, J. & Symes, W.W., 2002. An adaptive finite-difference method for traveltimes and amplitudes, *Geophysics,* **67,** 167–176.

Rawlinson, N. & Sambridge, M., 2004. Wave front evolution in strongly heterogeneous layered media using the fast marching method. *Geophys. J. Int.,* **156**(3), 631–647.

Sambridge, M., 1990. Non-linear arrival time inversion: constraining velocity anomalies by seeking smoothing models in 3-D, *Geophys. J. Int.,* **102,** 653–677.

Sehudandi, C. & Toint, P.L., 1993. Non-linear optimization for seimic traveltime tomography, *Geophys. J. Int.,* **105,** 929–940.

Sethian, J.A. & Popovici, A.M., 1999. 3-D traveltime computation using the fast marching method, *Geophysics,* **64,** 516–523

Shearer, P.M. & Chapman, C.H., 1988. Ray tracing in anisotropic media with a linear gradient, *Geophys. J. Int.,* **94,** 575–580.

Takeuchi, H. & Satio, M., 1972. Seismic surface wave, *Methods Comput. Phys.,* **11,** 217–295.

Tanimoto, T. & Anderson, D.L., 1985. Materal heterogeneity and azimuthal anisotropy of the upper mantle: Love and Rayleigh waves 100–200s, *J. geophys. Res.,* **90,** 1842–1858.

Tarantola, A., 1984. Inversion of seismic reflection reflection data in the acoustic approximation, *Geophysics,* **49,** 1259–1266.

Tarantola, A., 1987. *Inverse Problem Theory, Methods for Data Fitting and Model Parameter Estimation*, Elsevier, Amsterdam.

Thomsen, L., 1986. Weak elastic anisotropy, *Geophysics,* **51,** 1954–1966.

Tsvankin, I. & Grechka, V., 2006. Development in seismic anisotropy: treating realistic subsurface models in imaging and fracture detection, *CSEG RECORDER*, 43–46.

Vavryčuk, V., 2001. Ray tracing in anisotropic media with singularities, *Geophys. J. Int.,* **145,** 265–276.

Vidale, J.E., 1990. Finite-difference calculation of travel time in three dimensions, *Geophysics,* **55,** 521–526.

Watanabe, T., Hirai, T. & Sassa, K., 1996. Seismic traveltime tomography in anisotropic heterogeneous media, *J. Appl. Geophys.,* **35,** 133–143.

Wu, H. & Lees, J.M., 1999. Cartesian parameterization of anisotropic traveltime tomography, *Geophys. J. Int.,* **137,** 64–80.

Xu, K., Greenhalgh, S.A. & Wang, M., 2006. Comparison of source-independent methods of elastic waveform inversion, *Geophysics,* **71,** R91-R100.

Zelt, B.C., Ellis, R.M., Zelt, C.A., Hyndman, R.D., Lowe, C., Spence, G.D. & Fisher, M.A., 2001. Three-dimensional crustal velocity structure beneath the Strait of Georgia, British Columbia, *Geophys. J. Int.,* **144,** 695–712.

Zheng, X., 2004. Inversion for elastic parameters in a weakly anisotropic medium, *Geophys. J. Int.,* **159,** 1077–1089.

Zhou, B. & Greenhalgh, S.A., 2004. On the computation of elastic wave group velocity for a general anisotropic medium, *J. geophys. Eng.,* **1,** 205–215.

Zhou, B. & Greenhalgh, S.A., 2005a. Analytic expressions for the velocity sensitity to the elastic moduli for the most general anisotropic media, *Geophys. Prospect.,* **53,** 619–641.

Zhou, B. & Greenhalgh, S.A., 2005b. 'Shortest path' ray tracing for the most general anisotropic 2D/3D anisotropic media, *J. geophys. Eng.,* **2,** 54–63.

Zhou, B., Greenhalgh, S.A. & Sinadinoviski, C., 1992. Iterative algorithm for the damped minimum norm, least-squares and constrained problem in seismic tomography, *Explor. Geophys.,* **23,** 497–505.